

# Single crystal EPR spectroscopy, magnetic studies and catalytic activity of a self-assembled $[2 \times 2]$ $\text{Cu}_4^{\text{II}}$ cluster obtained from a carbohydrazone based ligand



Rahman Bikas<sup>a,\*</sup>, Hassan Hosseini-Monfared<sup>a</sup>, Pavlo Aleshkevych<sup>b,\*</sup>, Ritta Szymczak<sup>b</sup>, Milosz Siczek<sup>c</sup>, Tadeusz Lis<sup>c</sup>

<sup>a</sup> Department of Chemistry, Faculty of Science, University of Zanjan, 45371-38791 Zanjan, Iran

<sup>b</sup> Institute of Physics, Polish Academy of Sciences (PAN), Al. Lotnikow 32/46, PL-02-668 Warsaw, Poland

<sup>c</sup> Faculty of Chemistry, University of Wrocław, Joliot-Curie 14, 50-383 Wrocław, Poland

## ARTICLE INFO

### Article history:

Received 27 September 2014

Accepted 28 November 2014

Available online 27 December 2014

### Keywords:

Single crystal EPR  
Magnetic studies  
Catalytic epoxidation  
 $[2 \times 2]$   $\text{Cu}_4^{\text{II}}$  cluster  
Exchange coupling

## ABSTRACT

A new tetranuclear  $[2 \times 2]$  cluster of Cu(II) with a symmetric carbohydrazone based ligand,  $[\text{Cu}_4\text{L}_4](\text{NO}_3)_4 \cdot 1.6(\text{H}_2\text{O})$  (**1**), {where HL donates bis-[(*E*)-*N'*-(1-(pyridin-2-yl)ethylidene)]carbohydrazone} was synthesized and characterized by spectroscopic methods and X-ray analysis. The EPR spectra were performed on single crystals of complex **1** at various temperatures and allowed the identification and separation of two types of magnetic objects contributing to magnetism: single atoms of Cu(II) and a tetranuclear  $\text{Cu}_4$  cluster. The main values of the *g*-factor and hyperfine structure were determined for single ions of Cu(II). The copper atoms in the tetramer are coupled antiferromagnetically with an isotropic antiferromagnetic exchange  $J = 215 \text{ K}$  ( $149.4 \text{ cm}^{-1}$ ). A small anisotropic exchange of the order of  $0.06 \text{ K}$  ( $0.04 \text{ cm}^{-1}$ ) is responsible for the initial zero-field splitting of the energy levels in the tetramer spectrum. Magnetic measurements of complex **1** confirmed the existence of a strong antiferromagnetic exchange coupling between four Cu(II) ions. Complex **1** showed high potential for the catalytic and selective oxidation of *cis*-cyclooctene with aqueous  $\text{H}_2\text{O}_2$ .

© 2014 Elsevier Ltd. All rights reserved.

## 1. Introduction

The construction of multinuclear transition metal complexes (MTMCs) remains a popular research area in the field of coordination and material chemistry [1]. This is mainly due to the peculiar structure diversity of MTMCs and their potential application as functional materials in fields such as catalysis [2], photochemistry [3], ion exchange [4], sensor technology [5] and magnetic materials [6]. In recent years polynuclear  $[2 \times 2]$ ,  $[3 \times 3]$  and  $[n \times n]$  molecular grid systems containing conformationally rigid tetranuclear macrocyclic ring systems with approximately  $90^\circ$  bond angles about each metallic corner have attracted the eyes of various research groups [7]. Some of these clusters show strong magnetic interactions and single molecule magnet (SMM) behavior [8]. In this context, copper(II) complexes are of particular interest because of the flexible coordination sphere of the Cu(II) ion and the versatile applications of its complexes in various fields such

as magnetism [9], biology [10] and medicine [11]. As catalysts, for example, Cu(II) complexes show catalytic activities for the epoxidation of olefins [12], oxidation of alkanes [13], sulfoxidation [14], cycloaddition [15] and polymerization reactions [16].

The controlled preparation of MTMCs with pre-established structures, properties and functions is one of the challenges in synthetic coordination chemistry. Among the various strategies for the design of MTMCs, the self-assembly reaction between metal sources and specifically designed precursors may lead to various interesting polynuclear structures [17]. However, the self-assembly of materials for this kind of complex does not occur by chance and requires structural specificity together with particular multi-dentate ligands [18]. The structure of the ligand plays the most important role in the construction of MTMCs [19]. Some hydrazone based ligands bearing multi-dentate donor atoms in specific regions are good candidates for the design of grid-like metal ion arrays, and  $[4 \times 4]$  and  $[3 \times 3]$  grid networks of Cu(II) have been reported by a symmetric multidentate hydrazone ligand [20]. Carbohydrazone based ligands are a special type of symmetric ligand in the hydrazone family which are ideal precursors for the design of  $[2 \times 2]$  clusters. Surprisingly, however, there are a few reports

\* Corresponding authors. Tel.: +98 241 5152576; fax: +98 241 2283203 (R. Bikas).

E-mail addresses: [bikas@znu.ac.ir](mailto:bikas@znu.ac.ir), [bikas\\_r@yahoo.com](mailto:bikas_r@yahoo.com) (R. Bikas), [pavloa@ifpan.edu.pl](mailto:pavloa@ifpan.edu.pl) (P. Aleshkevych).

including Fe [21], Cd [22], Zn [23] and Co [24] examples concerning structural characterization of this type of system. Recently, it has been reported that lanthanide complexes of carbohydrazone based ligands show SMM behavior [25]. To the best of our knowledge and according to the reported structures in the Cambridge Structural Database (CSD) [26], there are no reports regarding the structures of  $[2 \times 2]$  Cu complexes using symmetric hydrazone ligands. Furthermore, understanding the magnetic interactions in novel  $[2 \times 2]$  clusters with symmetric ligands will be interesting. The exchange clusters of magnetic ions in the MTMCs are the simplest ferromagnets or antiferromagnets where exchange interactions between a small numbers of magnetic ions has to be taken into account. On the other hand, their magnetic properties depend strongly on the symmetry and electronic nature of the magnetic ions and the structures of the nearest neighboring ligands. These factors strongly affect the EPR spectrum. The EPR technique is known to be a useful tool in the study of exchange clusters, ensuring its effectiveness because of the high sensitivity, selectivity and large analytical background accumulated over many decades of using EPR. In this article we report the synthesis, crystal structure, EPR spectrum, magnetic behavior and catalytic activity of a tetranuclear  $[2 \times 2]$  cluster of Cu(II) with a symmetric carbohydrazone based ligand. To achieve the full advantage of using EPR spectroscopy, the presented EPR study was performed on single crystals.

## 2. Experimental

### 2.1. Materials and instrumentations

All starting materials were purchased from Acros and used as received. Solvents of the highest grade commercially available (Merck) were used without further purification. IR spectra were recorded as KBr disks with a Bruker FT-IR spectrophotometer (model: TENSOR 27). UV–Vis spectra of solutions were recorded on a thermo spectronic, Helios Alpha spectrophotometer.  $^1\text{H}$  and  $^{13}\text{C}$  NMR spectra of the ligand in DMSO- $d_6$  solution were measured on a Bruker 250 MHz spectrometer and chemical shifts are indicated in ppm relative to tetramethylsilane. The atomic absorption analysis was carried out using Varian Spectra AA-220 equipment. The magnetic susceptibility and magnetization vs. magnetic field were measured with a Quantum Design SQUID MPMS XL magnetometer in a magnetic field up to 5 T and in the temperature range 2–300 K. The magnetic susceptibility measurements were carried out both in the zero-field-cooled (ZFC) and field-cooled (FC) modes. No differences between the ZFC and FC results and no magnetic phase transitions were observed. The EPR measurements were carried out using a Bruker EMX spectrometer working at a fixed frequency of 9.25 GHz (X-band) with an Oxford helium-flow cryostat instrument operating in the temperature range from 3.8 to 300 K. A 100 kHz magnetic field modulation and phase sensitive detection were used to record the derivative of the absorbed microwave power. The samples were maintained in a rotatable sample holder to record the angular variation of the EPR spectra.

### 2.2. Synthesis of bis-[(E)-N'-(1-(pyridin-2-yl)ethylidene)]carbohydrazone (HL)

A methanol (10 mL) solution of carbohydrazone (0.50 g, 5.55 mmol) was added dropwise to a methanol solution (10 mL) of 2-acetylpyridine (1.34 g, 11.10 mmol) and the mixture was refluxed for 6 h. The solution was evaporated on a steam bath to 5 mL and cooled to room temperature. The resulting white precipitate was separated and filtered off, washed with 5 mL of cooled methanol and recrystallized. Yield: 95% (1.56 g). *Anal. Calc.* for  $\text{C}_{15}\text{H}_{16}\text{N}_6\text{O}$  (MW = 296.33): C, 60.80; H, 5.44; N, 28.36. Found: C,

60.73; H, 5.46; N, 28.42%. FT-IR (KBr,  $\text{cm}^{-1}$ ): 3445 (m, br), 3355 (m), 3206 (m, N–H), 3061 (m), 2923 (m), 1700 (vs C=O), 1680 (vs), 1578 (m), 1518 (s), 1462 (s), 1433 (s), 1310 (w), 1261 (s), 1132 (s), 991 (w), 808 (m), 788 (s), 739 (m), 598 (w), 528 (w), 441 (w), 404 (w).  $^1\text{H}$  NMR (250.13 MHz, DMSO- $d_6$ , TMS)  $\delta$  (ppm): 10.87 (s, 2H, N–H), 8.61 (d, 2H,  $J = 7.25$  Hz), 8.12 (d, 2H,  $J = 7.5$  Hz), 7.91 (m, 2H), 7.43 (t, 2H,  $J = 7.5$  Hz), 2.45 (s, 6H).  $^{13}\text{C}$  NMR (250.13 MHz, DMSO- $d_6 + \text{D}_2\text{O}$ )  $\delta$  (ppm): 7.39–8.70 (10 H, aromatic), 2.59 (s, 6H).  $^{13}\text{C}$  NMR (62.90 MHz, DMSO- $d_6$ )  $\delta$  (ppm): 12.4, 120.8, 124.7, 136.4, 144.9, 149.1, 152.1, 157.3. UV–Vis (in  $\text{CH}_3\text{OH}$ ,  $c = 5 \times 10^{-5}$  mol  $\text{dm}^{-3}$ ,  $\lambda_{\text{max}}$  [nm] with  $\epsilon$  [ $\text{M}^{-1} \text{cm}^{-1}$ ]): 214 (33 000), 298 (36 000), 380<sup>sh</sup> (5600).

### 2.3. Synthesis of the complex $[\text{Cu}_4\text{L}_4](\text{NO}_3)_4 \cdot 1.6(\text{H}_2\text{O})$ (1)

The appropriate amount of the ligand HL (0.296 g, 1 mmol) was dissolved in methanol (30 mL) and  $\text{Cu}(\text{NO}_3)_2 \cdot 3\text{H}_2\text{O}$  (0.242 g, 1.00 mmol) was added. The solution was gently refluxed for 6 h. After cooling, the resulting solid was filtered off, washed with cooled absolute ethanol and dried at 100 °C. Purple crystals of **1** were prepared by slow solvent evaporation over one week. Yield 77% (0.33 g). *Anal. Calc.* for  $\text{C}_{60}\text{H}_{63.2}\text{Cu}_4\text{N}_{28}\text{O}_{17.6}$  (MW = 1712.34): C, 42.09; H, 3.72; N, 22.90; Cu, 14.84. Found: C, 41.95; H, 3.75; N, 22.86; Cu, 14.78%. FT-IR (KBr,  $\text{cm}^{-1}$ ): 3413 (m, br), 3058 (w), 1622 (m), 1601 (m), 1573 (s), 1548 (s), 1469 (m), 1384 (vs), 1353 (m), 1267 (m), 1155 (s), 1088 (m), 1011 (m), 789 (m), 775 (m), 699 (w), 570 (w), 403 (w). UV–Vis (in  $\text{CH}_3\text{OH}$ ,  $c = 2.5 \times 10^{-5}$  mol  $\text{dm}^{-3}$ ,  $\lambda_{\text{max}}$  [nm] with  $\epsilon$  [ $\text{M}^{-1} \text{cm}^{-1}$ ]): 221 (100 800), 369 (60 600), 470 (32 200), 695 (500).

### 2.4. X-ray crystallography

A summary of the crystal data and refinement details for complex **1** are given in Table 1. Only special features of the analyses are

**Table 1**  
Crystallographic data of **1**.

	Complex <b>1</b>
Net formula	$\text{C}_{60}\text{H}_{60}\text{Cu}_4\text{N}_{24}\text{O}_4(\text{NO}_3)_4 \cdot 1.6(\text{H}_2\text{O})$
$M_r$ ( $\text{g mol}^{-1}$ )	1712.34
Crystal size (mm)	$0.25 \times 0.20 \times 0.15$
Crystal shape	block
Color	purple
$T$ (K)	100(2)
Radiation ( $\text{\AA}$ )	Mo $K\alpha$ (0.71073)
Diffractometer	Xcalibur PX with Onyx CCD
Crystal system	tetragonal
Space group	$I4_1/a$
$a, b$ ( $\text{\AA}$ )	13.929(3)
$c$ ( $\text{\AA}$ )	35.16(2)
$V$ ( $\text{\AA}^3$ )	6822(5)
$Z$	4
$D_{\text{calc}}$ ( $\text{g cm}^{-3}$ )	1.667
$\mu$ ( $\text{mm}^{-1}$ )	1.32
Absorption correction	analytical
Reflections measured	33 214
$R_{\text{int}}$	0.027
$h, k, l$	$-19 \rightarrow 19, -14 \rightarrow 19, -50 \rightarrow 50$
$\theta$ range	$2.9\text{--}30.6$
Observed reflections	5242
Hydrogen refinement	mixed
Reflections in refinement	4003
Parameters/restraints	297/18
$F(000)$	3504
$R(F_{\text{obs}})$	0.028
$R_w(F^2)$	0.081
$S$	1.03
Shift/error <sub>max</sub>	0.001
Maximum/minimum electron density	0.39/−0.29
( $\text{e \AA}^{-3}$ )	

mentioned here. Single crystal data collection for **1** was performed on an Xcalibur PX diffractometer with an Onyx CCD detector, equipped with an Oxford Cryosystems open-flow nitrogen cryostat, using  $\omega$  scans and graphite-monochromated Mo K $\alpha$  ( $\lambda = 0.71073$  Å) radiation. The structure was solved by direct methods with SHELXS-97 [27], and refined with full-matrix least-squares techniques on  $F^2$  with SHELXL-97 [28]. The C-bonded hydrogen atoms were calculated in an idealized geometry riding on their parent atoms. The O and N-bonded hydrogen atoms were located from the difference map. The molecular structure plot was prepared using Diamond [29].

### 2.5. General oxidation procedure

Liquid phase catalytic oxidation of *cis*-cyclooctene was carried out under air (atmospheric pressure) in a 25 mL round bottom flask equipped with a magnetic stirrer. In a typical experiment, H<sub>2</sub>O<sub>2</sub> was added to a flask containing the catalyst (1  $\mu$ mol) and *cis*-cyclooctene (1 mmol) in solvent (3 mL). The course of the reaction was monitored using a gas chromatograph equipped with a capillary column and a flame ionization detector. The oxidation products were identified by comparing their retention times with those of authentic samples or alternatively by <sup>1</sup>H NMR and GC-Mass analyses. Control reactions were carried out in the absence of catalyst, under the same conditions as the catalytic runs. No products were detected.

## 3. Results and discussion

### 3.1. Synthesis and spectroscopy

The reaction of carbohydrazone with 2-acetylpyridine in methanol gave the desired symmetric Schiff base ligand, HL, in excellent yield and purity (Scheme 1). Keto-enol tautomerism of the arylhydrazone HL is illustrated in Scheme 1b. IR and NMR spectra of the ligand confirmed the proposed structure and indicate that the free ligand is stable in the keto form. In the <sup>1</sup>H NMR spectrum of the ligand the presence of a signal at  $\delta$  10.87 ppm was assigned to the common N-H group, which was consistent with the observation of a rapid loss of this signal when D<sub>2</sub>O was added to the solution. The aromatic hydrogen atoms appear at  $\delta$  7.4–8.6 ppm and the methyl hydrogens are located at  $\delta$  2.45 ppm. The IR spectrum of HL displays a characteristic band at 3206 cm<sup>-1</sup> which is due to  $\nu$ (N-H). In the IR spectrum of HL two strong bands appear at 1700 and 1680 cm<sup>-1</sup> due to  $\nu$ (C=O) stretching vibrations. Complex **1** was synthesized by the reaction of Cu(NO<sub>3</sub>)<sub>2</sub>·3H<sub>2</sub>O and HL in equimolar ratios, with methanol as the solvent. A comparison of the IR spectrum of complex **1** with that of the free ligand provides evidence for the coordination mode of HL. Elimination of the C=O

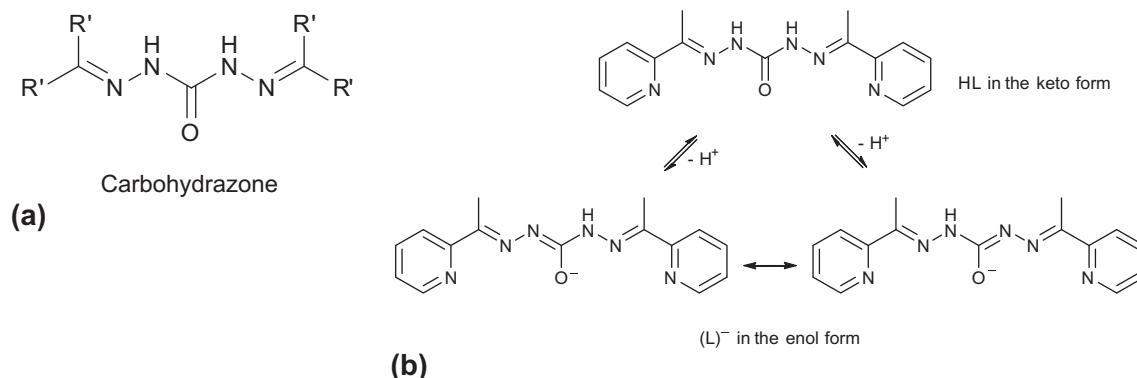
band is seen in the IR spectrum of the complex, which suggests enolization of the amide functionality of (L)<sup>-</sup> upon coordination to the metal ions. This finding is also confirmed by the appearance of a new band at 1622 cm<sup>-1</sup>, which may be assigned to the -C=N-N=C- moiety [30]. There is a weak band at 3058 cm<sup>-1</sup> in the IR spectrum of the complex, which is due to the presence of an N-H bond in **1** and indicates that one of the amidic hydrogen atoms of (L)<sup>-</sup> remains intact during the complexation. The disappearance of the carbonyl stretching vibration band and the presence of the N-H band suggests the absence of delocalization in the -N-C=O group in the coordinated (L)<sup>-</sup> ligand [31]. A broad absorption band at 3413 cm<sup>-1</sup> (O-H stretching) in the infrared spectrum of **1** is due to the presence of uncoordinated solvents.

The electronic spectra of complex **1** (green solution) and HL (colorless solution) in a MeOH solution are shown in Fig. S1. The hydrazone ligand displays strong bands at 214, 298 and 380 nm. Based on their extinction coefficients, they are assigned to intraligand  $\pi \rightarrow \pi^*$  (214, 298 nm) and  $n \rightarrow \pi^*$  (380 nm) transitions. Shifts and changes of the bands in the UV-Vis spectrum of the complex relative to the HL bands indicate the coordination of the ligand to the Cu(II) ions. For the complex, the higher energy bands at 369 and 470 nm, with high extinction coefficient values, are due to ligand to metal charge transfer (LMCT) transitions. The other higher energy intense transition at 221 nm is assigned to the intraligand  $\pi \rightarrow \pi^*$  charge transfer transitions. The band for the d-d transition appears as a broad weak peak near 700 nm.

### 3.2. X-ray structure of [Cu<sub>4</sub>(L)<sub>4</sub>](NO<sub>3</sub>)<sub>4</sub>·1.6(H<sub>2</sub>O) (**1**)

The structure of complex **1** and the coordination core about the Cu(II) centers with selected bond lengths and angles are given in Fig. 1. The core of the tetranuclear compound is composed of four symmetry-related copper(II) ions, creating an almost square geometry with a slight deformation towards a tetrahedral geometry. Distortion from planarity can be noted in the value of the deviation from the best plane created by the four copper atoms, which is perpendicular to the fourfold inversion axis (Fig. 1b). Two Cu atoms are above the best plane by 0.2791(1) Å and the other two are below the plane by -0.2791(1) Å.

The tetranuclear Cu<sub>4</sub>L<sub>4</sub><sup>4+</sup> [2 × 2] cation has four Cu(II) centers, to which the ligands are coordinated in the mononegative form, (L)<sup>-</sup>, by deprotonation of one N-H moiety. Four nitrate anions and H<sub>2</sub>O molecules surround the cation. Complex **1** crystallized in the I4<sub>1</sub>/a space group and is isomorphous to a zinc complex with another type of carbohydrazone based ligand [22]. The complex cation as a whole has S<sub>4</sub> symmetry. In the tetranuclear Cu<sub>4</sub>L<sub>4</sub> [2 × 2] unit, each Cu(II) atom is six-coordinated by two pyridyl nitrogen, two azomethine nitrogen and two enolate oxygen atoms. The overall geometry around the copper(II) ion is best described as a distorted



Scheme 1. (a) General formula of carbohydrazones and (b) the tautomeric forms of HL.

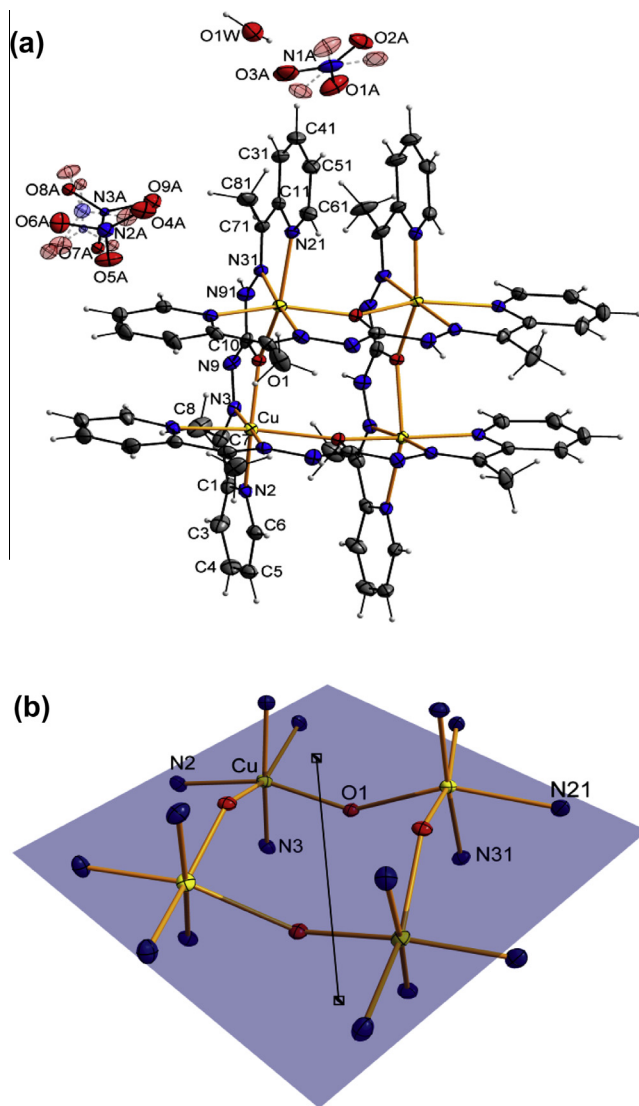


**Fig. 1.** (a) Molecular structure of complex **1** together with the numbering scheme; (b) coordination environment around the metal cores which are placed alternatively above and below the plane perpendicular to the fourfold inversion axis. Selected bond lengths (Å) and angles ( $^{\circ}$ ): Cu–N3 = 1.9415(17); Cu–N31<sup>i</sup> = 2.0119(17); Cu–O1 = 2.0261(10); Cu–O1<sup>i</sup> = 2.2933(10); Cu–N2 = 2.0340(13); Cu–N21<sup>i</sup> = 2.2535(13); O1–Cu–O1<sup>i</sup> = 91.03(5); N3–Cu–O1 = 78.98(5); N31<sup>i</sup>–Cu–O1 = 99.23(4); N3–Cu–N2 = 79.79(5); N31<sup>i</sup>–Cu–N2 = 102.37(5); O1–Cu–N2 = 157.77(5); N31<sup>i</sup>–Cu–N21<sup>i</sup> = 75.61(5); O1–Cu–N21<sup>i</sup> = 91.76(4); N2–Cu–N21<sup>i</sup> = 98.63(5); N21<sup>i</sup>–Cu–O1<sup>i</sup> = 150.09(4) where  $i = -y + 5/4, x + 1/4, -z + 1/4$ .

octahedron with axial elongation due to the Jahn–Teller effect. Each (L)<sup>−</sup> ligand binds to two Cu(II) cations, in which the oxygen atom shares coordination to adjacent Cu(II) ions. These alternate copper and oxygen atoms form a boat–boat conformation [32] with an eight atom ring (Fig. 1b). Around each Cu(II) core, the two enolate O atoms and two pyridyl N atoms are located *cis* with respect to each other, whereas the azomethine N atoms are *trans*. The adjacent Cu··Cu distance is 4.070(1) Å and the Cu–O–Cu angle is 140.76(5) $^{\circ}$ , values which are close to other reported tetranuclear copper complexes with asymmetric hydrazone ligands [33]. The Cu··Cu distances across the diagonals are 5.701(1) Å and the Cu··Cu··Cu angles are 88.922(5) $^{\circ}$ .

The Cu–O and Cu–N distances are close to those found in other Cu(II) complexes with N<sub>2</sub>O-donor hydrazone ligands [33]. The axial Cu–O1<sup>i</sup> and Cu–N21<sup>i</sup> bond distances are 2.2933(10) and 2.2535(13) Å, respectively. These two bonds are considerably elongated with respect to the other four, which is consistent with the

Jahn–Teller effect usually found in octahedral Cu(II) complexes with a d<sup>9</sup> electronic configuration [34].

Having H<sub>2</sub>O, NO<sub>3</sub><sup>−</sup> and amidic nitrogen functionality, it is not surprising that the crystal packing of **1** is dominated by strong and directional hydrogen bonds. Water molecules and NO<sub>3</sub><sup>−</sup> anions form a 1D polymeric chain through O–H··O hydrogen bonds. Also, there are strong C–H··π and π··π interactions between the pyridine rings [35] of the tetranuclear units. Some of these interactions are shown in Fig. S2. Geometric parameters characterizing the intermolecular interactions and hydrogen bonding connections are collected in Table S1.

### 3.3. EPR spectrum

Examples of resonance spectra obtained for single crystals of complex **1** recorded between 10 K and room temperature are shown in Fig. 2. At low temperatures ( $T < 30$  K) the spectra consist of groups of four intense equidistant lines associated with a single Cu(II) ion. The intensity of these lines decreases monotonically upon increasing the temperature, until they completely disappear at around 100 K. In the region of about 40–50 K new resonance lines become visible. These lines are labelled as (1)–(4) in Fig. 2 and their intensities show non-monotonic behavior versus temperature. It indicates that these lines belong to the exchange coupled complex, while the four lines in the low temperature region are due to isolated Cu(II) ions, with a clearly seen hyperfine structure.

The temperature dependencies of the integral intensities of all the resonance lines are shown in Fig. 3. The open square symbol shows the total intensity of the four lines of single Cu(II) ions, which follows a Curie-like temperature dependence. On the other hand, lines (1)–(4) change non-monotonically with temperature. Line (1) intensity at ~115 K, lines (2) and (3) each reach a maximum at ~125 K, while line (3) reaches a maximum at ~200 K. The solid circles represent the total intensity of all the resonance lines. The presence of a maximum for the temperature dependence of intensity indicates that the corresponding resonance transition occurs between energy levels far above the non-magnetic ground state, and thus is thermally activated. Based on the crystallographic data and stoichiometry in the single crystals of complex **1**, it is anticipated that the observed resonance lines (1)–(4) originate from antiferromagnetically coupled  $\overline{\text{Cu-Cu-Cu-Cu}}$  tetramers, with no exchange between the different tetramers. According to the structure, the four Cu(II) atoms almost form a square with a Cu··Cu distance equal to 4.070(1) Å. The local environment of each of the four Cu(II) atoms is identical, as well as the nature of the bridging chemical parts between nearest neighboring Cu(II) atoms. These data allow the assumption that in the first approach, and to avoid over parametrization, each of the nearest Cu–Cu pairs is characterized by the same exchange coupling and the following spin-Hamiltonian can be used to explain the EPR results:

$$\hat{H} = \sum_{i=1}^4 \mu_B \vec{H} \vec{g}_i \hat{S}_i + \vec{S}_1 \vec{J} \vec{S}_2 + \vec{S}_1 \vec{J} \vec{S}_4 + \vec{S}_2 \vec{J} \vec{S}_3 + \vec{S}_3 \vec{J} \vec{S}_4 \quad (1)$$

where  $\mu_B$  is the Bohr magneton,  $\vec{H}$  – the external magnetic field vector,  $\hat{S}_i$  – the spin operator,  $\vec{g}_i$  – the *g*-tensor of a particular Cu(II) atom within the tetramer molecule,  $\vec{J}$  – the second rank dyadic tensor containing all the relevant exchange parameters involved in the bilinear exchange. The schematic positions of spins 1–4 forming the tetramer are shown in Fig. 4. For the EPR measurements and analysis of the spectra, the Cartesian axis system (*X,Y,Z*) was defined such that the axis *Z* is parallel to the fourfold inversion axis of the tetramer complex. The principal values of the *g*-tensors for each of the four Cu(II) atoms are assumed to be the same, but with different orientations of the principal magnetic axes. The Cartesian local site axis system for each of the four Cu(II) atoms is defined

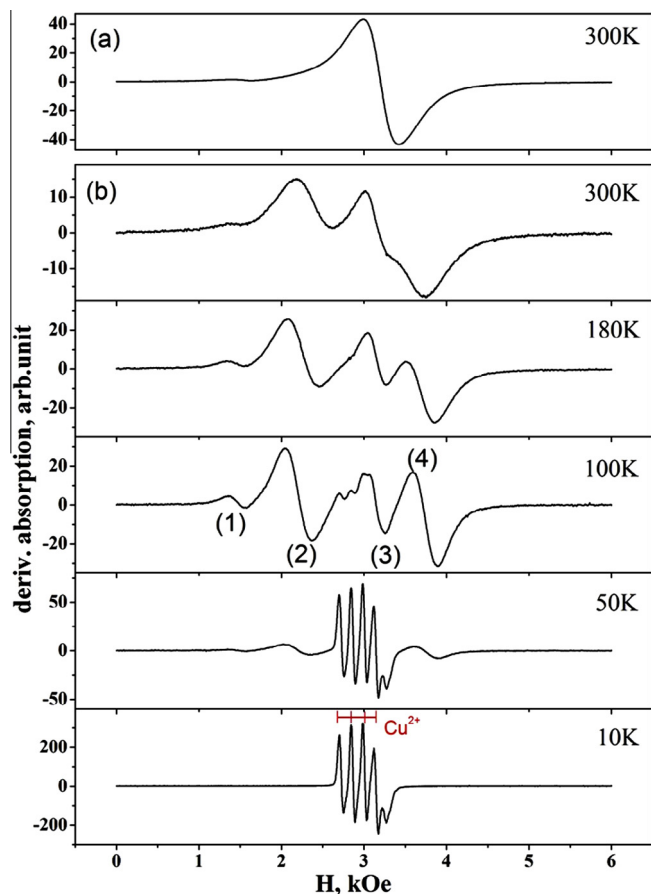


Fig. 2. Examples of the EPR spectra of single crystals of complex **1**, recorded at  $T = 10, 50, 100, 180, 300$  K with  $H$  parallel (a) and perpendicular (b) to the  $Z$  axis. The labels (1), (2), (3), (4) mark resonance transitions of the  $\text{Cu}_4$  tetramer. The group of 4 lines at 10 K shows the hyperfine structure of single  $3d^9$  Cu(II) ions.

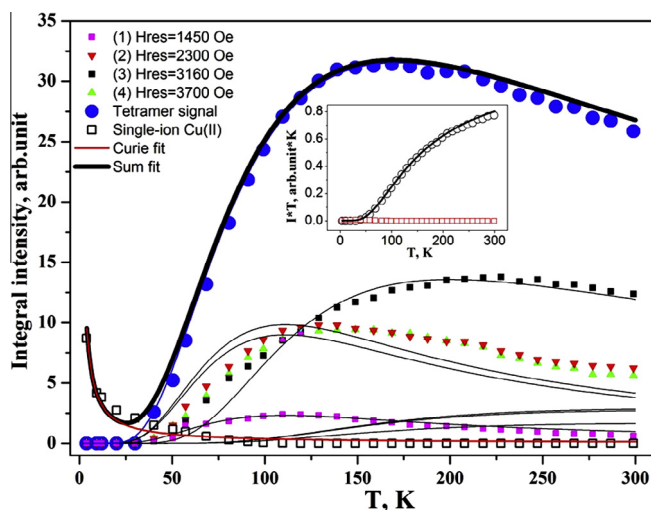
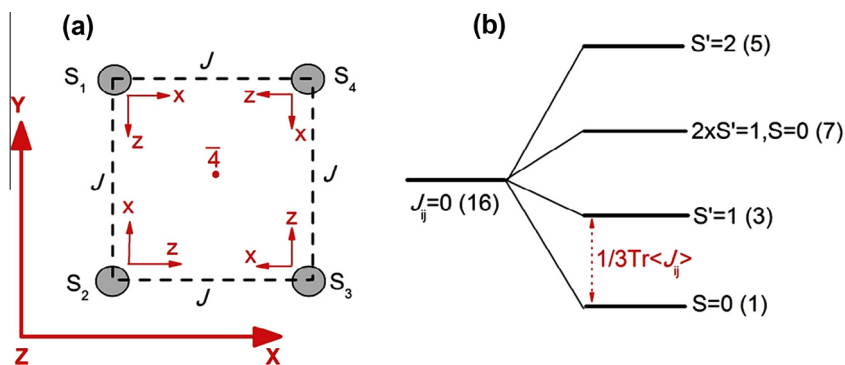


Fig. 3. The temperature dependencies of the integral intensities of all resolved resonance lines. The solid circles represent the total intensity of all the resonance lines. The solid lines show numerically calculated line intensities vs.  $T$  for transitions within different multiplets of the tetramer spectrum for  $J = 215$  K ( $149 \text{ cm}^{-1}$ ). The inset shows the product  $T \times \text{Intensity}$  vs.  $T$  for isolated Cu(II) (open square) and the sum of the tetramer + Cu(II) intensities (open circle) and the best fit.

with respect to  $XYZ$ , as shown in Fig. 4a. The local  $z_i$  axes were chosen to be parallel to the most elongated  $\text{Cu-O1}^i$  and  $\text{Cu-N21}^i$  bonds in the nearest environment of the Cu atom. The local  $y_i$  axes

are parallel to the  $Z$  axis. The magnetic coupling between the copper ions is mediated via the ligand bridges. It follows from the structure that there are no ligands connecting atoms through diagonals, therefore no cross-coupling is assumed. As any physical 2-rank tensor,  $\tilde{J}$  could be split into 3 parts,  $\tilde{J} = J\tilde{E} + \tilde{D} + \tilde{A}$ , where the isotropic part of the exchange interaction  $J = 1/3 \sum \text{Tr} \tilde{J} = 1/3(J_{xx} + J_{yy} + J_{zz})$ , the asymmetrical part  $A_{ij} = 1/2(J_{ij} - J_{ji})$  and the symmetrical part  $D_{ij} = 1/2(J_{ij} + J_{ji})$ , ( $E$  is the unity matrix and the elements of the tensor  $\tilde{J}$  are denoted as  $J_{ij}$ , where the sub indexes  $i, j = x, y, z$ ). The most meaningful influence on the magnetic properties of the tetramer comes from the diagonal elements of tensor  $\tilde{J}$  which are strictly related to the isotropic part of exchange interaction  $J$ . In the case of the tetramer, the isotropic exchange  $J$  splits 16-fold degenerated levels into four multiplets (see diagram in Fig. 4) [36]. For the anti-ferromagnetic interaction ( $J > 0$ ), the ground state is a singlet. The first excited multiplet is a triplet, which could be described by the effective spin  $S' = 1$ . The separation between the multiplets is proportional to the isotropic exchange  $J$ . The slight deviation from a square to the distorted  $\text{Cu}_4$  cluster does not change the multiplet splitting qualitatively, but may lift the degeneration of multiplets and could give rise to off-diagonal elements  $J_{ij}$ , where  $i \neq j$ . The  $J$  value can be found by analyzing the temperature dependence of the integral intensity of the resonance lines. To identify correctly the resonance transitions labelled as (1)–(4) on Fig. 2, the angular variation of the resonance spectrum was measured at 120 K in the  $XY$  plane (Fig. 5). As one can see, the positions of experimental lines (2) and (4) resemble the fine structure that could be described by an effective spin  $S' = 1$ . Additionally, line (1), located at the “half-field” position ( $H_{\text{res}} = 1440$  Oe), is a partially allowed transition within the same triplet involving a change of the electron magnetic quantum number by 2 ( $\Delta M_{S'} = 2$ ). The maximal intensity of lines (1), (2) and (4) occurs at the same temperature, therefore these resonance transitions belong to the same thermally activated spin triplet with  $S' = 1$ , which is the first excited multiplet of the tetramer. The line (3) apparently originates from higher multiplets as it has maximal intensity at nearly double the temperature ( $\sim 200$  K) as compared with the first excited multiplet.

The presence of fine structure indicates that the degeneracy of each of the multiplets is lifted because of zero-field splitting. Neither isotropic exchange nor a crystal field acting on Cu(II) can lift the degeneracy within the multiplets and explain the presence of the fine structure. We assume that the main contribution to the zero-field splitting is caused by small off-diagonal elements of tensor  $\tilde{J}$  ( $J_{ij}$ , with  $i \neq j$ ) related to anisotropic exchange [37]. The properly constructed spin Hamiltonian should be invariant upon the cluster point group symmetry transformation. Due to the high  $S_4$  symmetry of the  $\text{Cu}_4$  cluster, we assume that the antisymmetric part of the anisotropic exchange, related to Dzialoszyński–Moria interactions, is zero ( $J_{ij} - J_{ji} = 0$ ) and in the first approach every off-diagonal element of the elements of  $\tilde{J}$  can be reduced to the single parameter  $J_{ij} = J_{ji}$  ( $i < j$ ) =  $D$ , accounting for the symmetrical part of the anisotropic exchange. The exact numerical diagonalization of the spin-Hamiltonian (1) was used to calculate the resonance line positions by using a self-developed computer program. Using the least-square procedure, the program fits simultaneously only three spin-Hamiltonian parameters, i.e.  $g_x, g_z, D$ . This method implicitly assumes the coincidence of the principal axes of the  $g$ -tensor with the local site axis system for each Cu(II) atom. Of course, this assumption is not strictly valid for monoclinic or triclinic site symmetries. The calculated positions of eight resonance transitions within the tetramer spectrum are shown by solid lines in Fig. 5. The best agreement with the experimental positions of the resonance lines was achieved for  $g_x = 2.09 \pm 0.02$ ,  $g_z = 2.28 \pm 0.01$ ,  $D = 0.06 \pm 0.01$  K ( $0.04 \text{ cm}^{-1}$ ). The calculated resonance fields reproduce very well the experimental angular



**Fig. 4.** (a) The schematic representation of the  $\text{Cu}_4$  tetramer. The dashed lines connect spins coupled by  $J$ . The  $X, Y, Z$  axes are the spin-Hamiltonian (1) Cartesian axis system. The  $x, y, z$  axes are the local site axis system for each of the 4  $\text{Cu}(\text{II})$  atoms ( $y \parallel Z$ ). (b) The splitting of the 16-fold degenerated level of the tetramer under antiferromagnetic isotropic exchange. The numbers in round bracket show the degeneracy of the multiplets without a magnetic field. The splitting between the multiplets is proportional to the trace of the exchange coupling tensor  $\bar{J}$ .

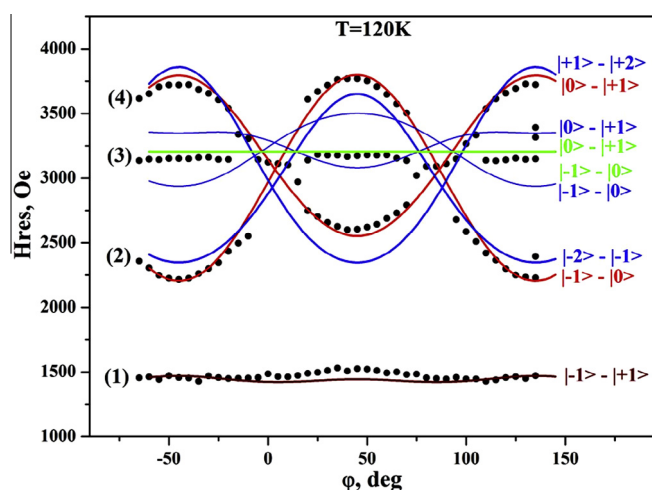


**Fig. 5.** The symbols represent the angular variations of the experimental resonance fields of lines measured at 120 K. The axis of rotation is the fourfold inversion axis of the tetramer. The labels (1)–(4) correspond to resonance lines shown in Fig. 3. The solid lines show the numerically calculated angular dependencies of the resonance transitions of the tetramer best fitted to experimental points for:  $g_x = 2.09 \pm 0.02$ ,  $g_z = 2.28 \pm 0.01$ ,  $D = 0.06 \pm 0.01$  K. The red, green and blue lines correspond to transitions from the first, second and third excited multiplet of the tetramer energy spectrum, respectively. On the right side there are identifications for each of the resonance transitions. (Color online.)

dependence. The experimental lines (2)–(4) are, in fact, the superposition of resonance transitions from different excited multiplets of the tetramer energy spectrum. Three resonance transitions within the first excited multiplet of the tetramer spectrum (labelled as  $S' = 1$  in Fig. 4b) are most intensive at  $T = 120$  K and are shown by red lines in Fig. 5. The green line describes the nearly isotropic allowed transitions ( $\Delta M_S' = 1$ ) within the second excited multiplet ( $2 \times S' = 1, S = 0$ ). There are also four transitions within the highest excited multiplet ( $S' = 2$ ), shown by blue solid lines. These transitions are still much less intensive at 120 K than transitions from lower excited multiplets. The fine structure at  $H \parallel Z$  is grouped into a poorly resolved resonance line (see spectrum in Fig. 2a) centered around  $H_{\text{res}} = 3200$  Oe, which gives us the missing value of  $g_y = 2.094 \pm 0.004$ . Therefore, within the errors of calculation, each of the  $\text{Cu}(\text{II})$  atoms are characterized by an axial  $g$ -tensor with two principal values  $g_x = g_y = g_{\perp} = 2.09$ ,  $g_{\parallel} = 2.28$ .

The intensity of the resonance transition  $I_{\text{pq}}$  between two energy levels  $E_p$  and  $E_q$  at a given temperature  $T$  was evaluated by the following general formula [38]:

$$I_{\text{pq}} = (H_{\text{pq}})^2 \frac{1}{\sum_i e^{\frac{E_i}{kT}}} \left[ e^{\frac{E_p}{kT}} - e^{\frac{E_q}{kT}} \right] \quad (2)$$

where  $H_{\text{pq}}$  is the matrix element corresponding to the transition  $I_{\text{pq}}$ . The summation in the denominator runs over all populated levels in the energy spectrum. Utilizing Eq. (2), the temperature dependencies of the resonance transition intensities from different multiplets of the tetramer as well as isolated  $\text{Cu}(\text{II})$  ions were calculated and are shown as solid lines in Fig. 3. For the single  $\text{Cu}(\text{II})$  ion, the intensity of one resonance transition, according to Eq. (2), is essentially simplified to Curie-like, inversely proportional to temperature dependence. The overall intensity was a weighted sum of the resonance lines of the tetramer and the isolated  $\text{Cu}(\text{II})$  ion:  $I_{\text{sum}} = (1 - \rho)I_{\text{tetramer}} + \rho I_{\text{Cu}(\text{II})}$ . A good agreement between the experimental and calculated dependencies occurs for  $J = (215 \pm 15)$  K ( $149 \pm 12$   $\text{cm}^{-1}$ ) and the fraction of isolated  $\text{Cu}(\text{II})$  is  $\rho \approx (2.5 \pm 0.5)\%$ . The angular variation of the resonance fields of the isolated  $\text{Cu}(\text{II})$  ion at 30 K is shown in Fig. S3. As is seen, the dependence shows the hyperfine structure due to the nuclear spin  $I = 3/2$  of the  $3d^9$  electron configuration of the  $\text{Cu}(\text{II})$  ions. The experimental points could be described by close to axial anisotropy of both  $g$ -factor and hyperfine splitting parameters:  $g_{\perp} = 2.09 \pm 0.04$ ,  $g_{\parallel} = 2.28 \pm 0.05$ ,  $A_{\perp} = 0.0019 \pm 0.0004$   $\text{cm}^{-1}$ ,  $A_{\parallel} = 0.0156 \pm 0.0010$   $\text{cm}^{-1}$ . This small fraction of isolated  $\text{Cu}(\text{II})$  ions are uncontrolled impurities associated with microcrystallites of copper nitrate precipitated on the crystal faces.

### 3.4. Magnetic studies

Magnetic measurements of complex **1** confirm the existence of strong magnetic exchange coupling between four  $\text{Cu}(\text{II})$  ions, also observed by means of the EPR technique. The temperature dependent magnetic susceptibility of powdered crystals of the complex was examined on an MPMS-XL7 SQUID magnetometer over the temperature range 2–300 K. A plot of the molar magnetic susceptibility measured in magnetic field  $H = 6$  kOe and corrected for diamagnetic contributions and TIP is displayed in Fig. 6 in the form of  $\chi(T)$  and  $\chi T(T)$ . It is seen from this figure that at room temperature  $\chi T(T)$  is  $1.7$   $\text{cm}^{-3}$  K/mol, which is near (in the limit of experimental error) to the theoretical value calculated for Cu in the  $\text{Cu}_4$  unit ( $S = 1/2$  and  $g = 2.15$  from the EPR spectrum, which is considered as an average value of the parallel and perpendicular components of the anisotropic  $g$  tensor) without any interaction between ions. As the temperature is lowered,  $\chi T(T)$  keeps the continuous decrease, which is characteristic of antiferromagnetic coupling between magnetic centers.

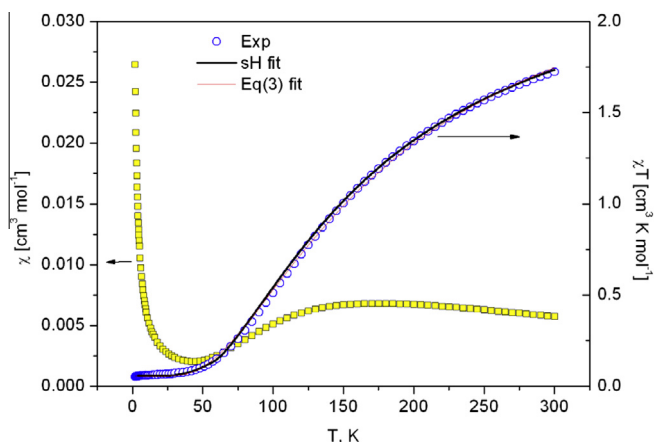


Fig. 6. Susceptibility  $\chi$  and  $\chi T$  vs. temperature. The solid lines present two theoretical calculations: using Eq. (3) and the spin-Hamiltonian (1).

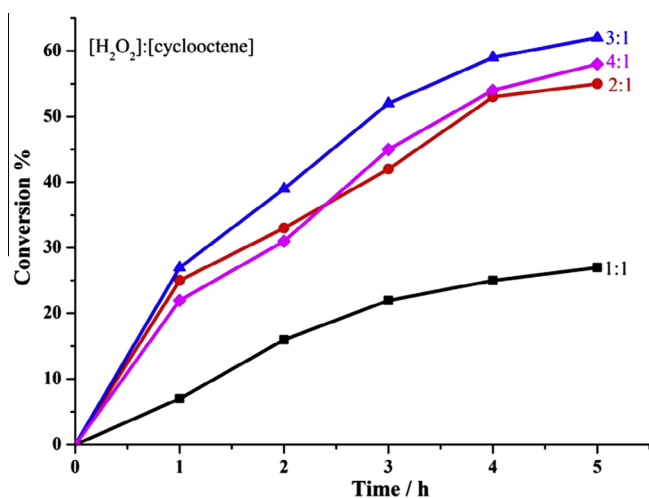


Fig. 7. Effect of  $\text{H}_2\text{O}_2$  concentration on the oxidation of cyclooctene by **1**. Reaction conditions: catalyst **1**, 1  $\mu\text{mol}$ ;  $\text{CH}_3\text{CN}$ , 3 mL; cyclooctene, 1 mmol; temperature, 60  $^\circ\text{C}$ .

In order to investigate quantitatively this coupling, an isotropic Heisenberg-Dirac-van Vleck (HDVV) Hamiltonian formalism was used (see eg., (1) in EPR analysis and also Ref. [39]). Since the bond

distances and bond angles in this tetranuclear unit are the same, the exchange interactions can be considered to be equivalent, and therefore  $J_1 = J_2 = J_3 = J_4 = J$  [39]. In the frame of this formalism the magnetic susceptibility may be expressed as [39]:

$$\chi_{\text{tetramer}} = (N_A (g\mu_B)^2 / (k_B T)) ((2e^{-J/T} + 4e^{-2J/T} + 10e^{-3J/T}) / (1 + 3e^{-J/T} + 7e^{-2J/T} + 5e^{-3J/T})),$$

$$\chi_{\text{total}} = (1 - \rho)\chi_{\text{tetramer}} + \rho 3/8g^2T \quad (3)$$

In this expression a Curie term is included in order to take into account a  $\rho\%$  fraction of monomeric Cu ions, suggested by EPR measurements. Using Eq. (3), the experimental data  $T\chi(T)$  were fitted in the temperature range 3–300 K with the best-fit parameters  $J \approx 234$  K (162  $\text{cm}^{-1}$ ),  $g = 1.91$  and  $\rho = 2.1\%$ . The obtained parameters  $J$  and  $g$  differ from those estimated from EPR data, because Eq. (3) accounts for the isotropic exchange only, without anisotropic exchange. Alternatively, the magnetic susceptibility was calculated numerically using the exact diagonalization of the spin-Hamiltonian (1) with  $J = 215$  K,  $D = 0.06$  K,  $\rho = 2.5\%$ ,  $g_{\perp} = 2.09$ ,  $g_{\parallel} = 2.28$ . After averaging between the three principal directions to approximate the powder behavior, the calculated  $\chi T$  value is shown in Fig. 6, labelled as “sH fit”. Both fits are in good agreement with the experimental data, but there is a more realistic value of the  $g$ -factor when a small anisotropic exchange is taken into account in the second case.

### 3.5. Catalytic activity

Since copper complexes of hydrazone ligands are good catalysts for the epoxidation of olefins [40], the catalytic activity of the complex was tested for the oxidation of *cis*-cyclooctene as a model substrate. In this regard, we were particularly interested to use the advantages of  $\text{H}_2\text{O}_2$  as a green and cheap oxidant. The catalytic oxidation of *cis*-cyclooctene was carried out with  $\text{H}_2\text{O}_2$  to give *cis*-cyclooctene oxide as the sole product. Control experiments revealed that the presence of oxidant and catalyst are essential for the oxidation.

To determine the optimal experimental conditions, the effects of  $\text{H}_2\text{O}_2$ /*cis*-cyclooctene molar ratio, the reaction temperature and influence of the solvent were studied. We have monitored the progress of *cis*-cyclooctene epoxidation for different molar ratios of oxidant and substrate. Molar  $\text{H}_2\text{O}_2$ /*cis*-cyclooctene ratios of 1, 2, 3 and 4 were considered, while keeping a fixed amount of *cis*-cyclooctene (1.0 mmol) and catalyst (1  $\mu\text{mol}$ ) in 3 mL of acetonitrile at 60  $^\circ\text{C}$  (Fig. 7). With a 1:1 ratio of  $\text{H}_2\text{O}_2$ :cyclooctene,

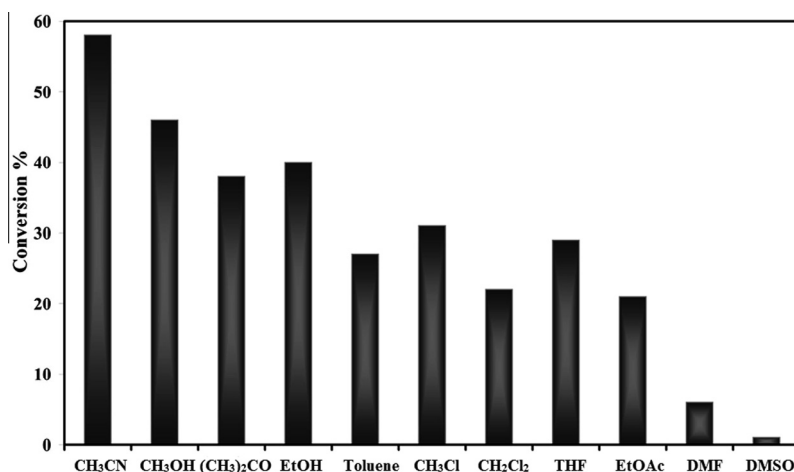
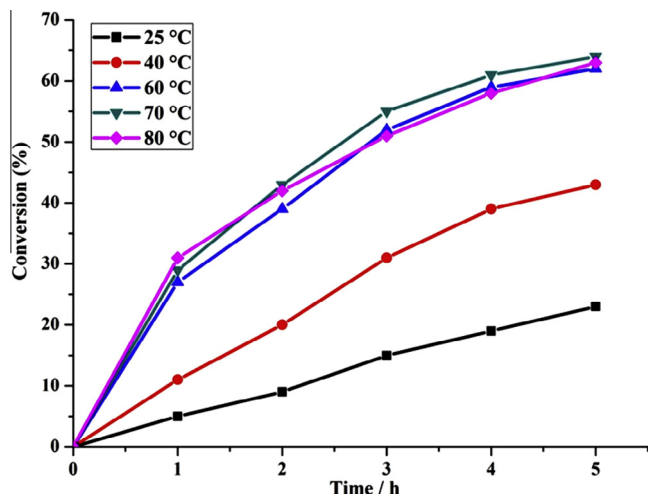


Fig. 8. Effect of solvent on the oxidation of cyclooctene by **1**. Reaction conditions: catalyst **1**, 1  $\mu\text{mol}$ ; solvent, 3 mL; cyclooctene, 1 mmol;  $\text{H}_2\text{O}_2$ , 3 mmol; temperature, 60  $^\circ\text{C}$ , time; 4 h.



**Fig. 9.** Effect of the reaction temperature on the oxidation of cyclooctene by **1**. Reaction conditions: Catalyst, complex **1**, 1  $\mu\text{mol}$ ;  $\text{CH}_3\text{CN}$ , 3 mL; cyclooctene, 1 mmol;  $\text{H}_2\text{O}_2$ , 3 mmol.

a conversion of up to 25% occurred after 4 h. Increasing the  $\text{H}_2\text{O}_2$ /*cis*-cyclooctene ratio to 2:1 and 3:1 increased the conversion to 55 and 62% after 5 h, respectively. Further increase of the ratio to 4:1 decreased the conversion to 58%. Hence, a  $\text{H}_2\text{O}_2$ /*cis*-cyclooctene ratio of 3:1 was selected for further studies.

**Fig. 8** illustrates the influence of the solvent in the catalytic oxidation of *cis*-cyclooctene. Methanol, ethanol, dichloromethane, chloroform, DMF, DMSO, THF and acetonitrile were used as solvents. Of the various solvents examined, acetonitrile was found to be the most suitable solvent for the reaction and is in agreement with activity of transition metal complexes of hydrazone ligands in oxidation reactions [41]. The highest conversion was obtained in acetonitrile after 4 h. It was observed that the catalytic activity of the catalyst decreased in the order acetonitrile > methanol > ethanol > acetone > chloroform > THF > toluene > dichloromethane > ethyl acetate > DMF > DMSO. Overall, the reactivity of the catalyst in other solvents was lower than in acetonitrile. The oxidation of *cis*-cyclooctene was also studied at 25, 40, 60, 70 and 80 °C. Increasing the reaction temperature up to 70 °C resulted in significantly higher yields of *cis*-cyclooctane epoxide (**Fig. 9**). In general, the catalytic reactivity of this complex is in the normal range reported for copper complexes of hydrazone ligands [40].

#### 4. Conclusion

In summary, a novel tetranuclear  $[2 \times 2]$  cluster of copper(II) has been synthesized and fully characterized by spectroscopic methods and X-ray analysis. The EPR spectra allowed the identification and separation of two types of magnetic objects contributing to the magnetism: single atoms of Cu(II) and a tetranuclear  $\text{Cu}_4$  cluster. The main values of the *g*-factor and hyperfine structure are determined for single ions of Cu(II). The copper atoms in the tetramer are coupled antiferromagnetically with an isotropic exchange  $J = 215 \text{ K}$  ( $149 \text{ cm}^{-1}$ ). The small anisotropic exchange of the order of 0.06 K ( $0.04 \text{ cm}^{-1}$ ) is responsible for the initial zero-field splitting of the energy levels in the tetramer's spectrum. Magnetic measurements of complex **1** confirm the existence of a strong antiferromagnetic exchange coupling between the four Cu(II) ions, also observed by means of the EPR technique. The catalytic reactivity of this complex for the oxidation of *cis*-cyclooctene was tested. This complex functions as an efficient and selective catalyst for the oxidation of *cis*-cyclooctene with aqueous  $\text{H}_2\text{O}_2$ .

#### Acknowledgments

The authors are grateful to the University of Zanjan and Institute of Physics, Polish Academy of Sciences for financial support of this study.

#### Appendix A. Supplementary data

CCDC 988074 contain the supplementary crystallographic data for complex **1**, respectively. These data can be obtained free of charge via <http://www.ccdc.cam.ac.uk/conts/retrieving.html>, or from the Cambridge Crystallographic Data Centre, 12 Union Road, Cambridge CB2 1EZ, UK; fax: (+44) 1223-336-033; or e-mail: [deposit@ccdc.cam.ac.uk](mailto:deposit@ccdc.cam.ac.uk). Supplementary data associated with this article can be found, in the online version, at <http://dx.doi.org/10.1016/j.poly.2014.11.038>.

#### References

- [1] Y. Lu, W. Chen, *Chem. Soc. Rev.* 41 (2012) 3594.
- [2] (a) K. Endo, M. Ogawa, T. Shibata, *Angew. Chem., Int. Ed.* 49 (2010) 2410; (b) Y. Hayashi, T. Ohshima, Y. Fujii, Y. Matsushima, K. Mashima, *Catal. Sci. Technol.* 1 (2011) 230.
- [3] (a) T. Morimoto, C. Nishiura, M. Tanaka, J. Rohacova, Y. Nakagawa, Y. Funada, K. Koike, Y. Yamamoto, S. Shishido, T. Kojima, T. Saeki, T. Ozeki, O. Ishitani, *J. Am. Chem. Soc.* 135 (2013) 13266; (b) F. Nastasi, M.L.D. Pietro, E. Trovato, F. Puntoriero, *Photochemistry* 41 (2013) 156.
- [4] (a) W.J. Chu, H.C. Yao, Y.T. Fan, H.W. Hou, *Dalton Trans.* 40 (2011) 2555; (b) H. Lü, Y. Mu, J. Li, D. Wu, H. Hou, Y. Fan, *Inorg. Chim. Acta* 387 (2012) 450.
- [5] (a) M.A. Rawashdeh-Omary, M.D. Rashdan, S. Dharanipathi, O. Elbejrani, P. Ramesh, H.V.R. Dias, *Chem. Commun.* 47 (2011) 1160; (b) G. Unden, S. Nilkens, M. Singenstreu, *Dalton Trans.* 42 (2013) 3082.
- [6] G. Aromí, D. Aguilà, P. Gamez, F. Luis, O. Roubeau, *Chem. Soc. Rev.* 41 (2012) 537.
- [7] (a) Y. Bi, W. Liao, X. Wang, X. Wang, H. Zhang, *Dalton Trans.* 40 (2011) 1849; (b) T.N. Mandal, S. Roy, S. Konar, A. Jana, S. Ray, K. Das, R. Saha, M.S. El Fallah, R.J. Butcher, S. Chatterjee, S.K. Kar, *Dalton Trans.* 40 (2011) 11866.
- [8] M.U. Anwar, L.N. Dawe, S.S. Tandon, S.D. Bunge, L.K. Thompson, *Dalton Trans.* 42 (2013) 7781.
- [9] (a) D. Draganca, S. Shova, É.A. Enyedy, M. Breza, P. Rapta, L.M. Carrella, E. Rentschler, A. Dobrov, V.B. Arion, *Polyhedron* 80 (2014) 180; (b) C.G. Efthymiou, C.P. Raptopoulou, V. Psycharis, A.J. Tasiopoulos, A. Escuer, S.P. Perlepes, C. Papatriantafyllopoulou, *Polyhedron* 64 (2013) 30; (c) J. Svorec, P. Polakovičová, J. Moncol, V. Kuchtanin, M. Breza, S. Šoralová, Z. Padělková, J. Mrozinski, T. Lis, P. Segla, *Polyhedron* 81 (2014) 216; (d) R. Bikas, H. Hosseini-Monfared, M. Korabik, M.S. Krawczyk, T. Lis, *Polyhedron* 81 (2014) 282; (e) H. Hosseini-Monfared, F. Mojtabazadeh, R. Bikas, V. Eigner, M. Dusek, A. Gutiérrez, *J. Coord. Chem.* 67 (2014) 3510.
- [10] A. Binolfi, L. Quintanar, C.W. Bertoncini, C. Griesinger, C.O. Fernández, *Coord. Chem. Rev.* 256 (2012) 2188.
- [11] (a) J.A. Drewry, P.T. Gunning, *Coord. Chem. Rev.* 255 (2011) 459; (b) C. Hureau, P. Dorlet, *Coord. Chem. Rev.* 256 (2012) 2175; (c) J.L. Hickey, P.S. Donnelly, *Coord. Chem. Rev.* 256 (2012) 2367.
- [12] M. Nandi, P. Roy, H. Uyama, A. Bhaumik, *Dalton Trans.* 40 (2011) 12510.
- [13] (a) A.M. Kirillov, M.V. Kirillova, A.J.L. Pombeiro, *Coord. Chem. Rev.* 256 (2012) 2741; (b) T.C.O. Mac Leod, M.N. Kopylovich, M.F.C. Guedes da Silva, K.T. Mahmudov, A.J.L. Pombeiro, *Appl. Catal. A* 440 (2012) 15.
- [14] H. Srour, P.L. Maux, S. Chevance, G. Simonneaux, *Coord. Chem. Rev.* 257 (2013) 3030.
- [15] (a) A. Sakakura, K. Ishihara, *Chem. Soc. Rev.* 40 (2011) 163; (b) Y.B. Cai, L. Liang, J. Zhang, H.L. Sun, J.L. Zhang, *Dalton Trans.* 42 (2013) 5390; (c) W.S. Brotherton, P.M. Guha, H. Phan, R.J. Clark, M. Shatruck, L. Zhu, *Dalton Trans.* 40 (2011) 3655.
- [16] S.O. Ojwach, T.T. Okemwa, N.W. Attandoh, B. Omondi, *Dalton Trans.* 42 (2013) 10735.
- [17] P.E. Kruger, T. Gunnlaugsson, *Dalton Trans.* 40 (2011) 12003.
- [18] (a) C.A. Palma, M. Cecchini, P. Samori, *Chem. Soc. Rev.* 41 (2012) 3713; (b) L.N. Dawe, K.V. Shuvaev, L.K. Thompson, *Chem. Soc. Rev.* 38 (2009) 2334.
- [19] (a) Z. Zheng, *Chem. Commun.* (2001) 2521; (b) M.D. Ward, P.R. Raithby, *Chem. Soc. Rev.* 42 (2013) 1619.
- [20] (a) L.N. Dawe, L.K. Thompson, *Angew. Chem., Int. Ed.* 46 (2007) 7440; (b) L.N. Dawe, K.V. Shuvaev, L.K. Thompson, *Inorg. Chem.* 48 (2009) 3323; (c) L.N. Dawe, T.S.M. Abedina, L.K. Thompson, *Dalton Trans.* (2008) 1661.
- [21] D.Y. Wu, O. Sato, Y. Einaga, C.Y. Duan, *Angew. Chem., Int. Ed.* 48 (2009) 1475.
- [22] X. Zhu, W. Huang, C. He, C.Y. Duan, *Chin. J. Inorg. Chem.* 26 (2010) 2138.
- [23] E.P. Manoj, M.R.P.P. Kurup, H.K. Fun, *Inorg. Chem. Commun.* 10 (2007) 324.

- [24] K. Shuvaev, L.N. Dawe, L.K. Thompson, *Dalton Trans.* 39 (2010) 4768.
- [25] M.U. Anwar, L.K. Thompson, L.N. Dawe, F. Habib, M. Murugesu, *Chem. Commun.* 48 (2012) 4576.
- [26] F.H. Allen, *Acta Crystallogr. B* 58 (2002) 380.
- [27] G.M. Sheldrick, *Acta Crystallogr. A* 64 (2008) 112.
- [28] G.M. Sheldrick, *SHELXS/L-97 Programs for Crystal Structure Determination*, University of Göttingen, Göttingen, Germany, 1997.
- [29] Brandenburg, K. *Diamond (Version 3.2d)*, Crystal and Molecular Structure Visualization, Crystal Impact – K. Brandenburg & H. Putz Gbr, Bonn (Germany), (2009).
- [30] (a) R. Bikas, H. Hosseini-Monfared, V. Vasylyeva, J. Sanchiz, J. Alonso, J.M. Barandiaran, C. Janiak, *Dalton Trans.* 43 (2014) 11925;  
(b) R. Bikas, H. Hosseini-Monfared, G. Zoppellaro, R. Herchel, J. Tucek, A.M. Owczarzak, M. Kubicki, R. Zboril, *Dalton Trans.* 42 (2013) 2803;  
(c) R. Bikas, H. Hosseini-Monfared, T. Lis, M. Siczek, *Inorg. Chem. Commun.* 15 (2012) 151;  
(d) H. Hosseini-Monfared, R. Bikas, M. Siczek, T. Lis, R. Szymczak, P. Aleshkevych, *Inorg. Chem. Commun.* 35 (2013) 172;  
(e) H. Hosseini-Monfared, R. Bikas, J. Sanchiz, T. Lis, M. Siczek, J. Tucek, R. Zboril, P. Mayer, *Polyhedron* 61 (2013) 45;  
(f) H. Hosseini-Monfared, R. Bikas, S. Mohammadi, T.M. Percino, S. Demeshko, F. Meyer, M.A.L. Ramirez, *Z. Anorg. Allg. Chem.* 640 (2014) 405.
- [31] (a) H. Hosseini-Monfared, H. Falakian, R. Bikas, P. Mayer, *Inorg. Chim. Acta* 394 (2013) 526;  
(b) R. Bikas, H. Hosseini-Monfared, M. Siczek, A. Gutiérrez, M.S. Krawczyk, T. Lis, *Polyhedron* 67 (2014) 396.
- [32] (a) J. Perez, L. Garcia, M. Kessler, K. Nolsøe, E. Perez, J.L. Serrano, J.F. Martinez, R. Carrascosa, *Inorg. Chim. Acta* 358 (2005) 2432;  
(b) H. Fuhrer, H. Meier, G. Rist, S.D. Pastor, S.P. Shum, F.H. Clarke, *Helv. Chim. Acta* 76 (1993) 1476;  
(c) S. Norrehed, M. Erdélyi, M.E. Light, A. Gogoll, *Org. Biomol. Chem.* 11 (2013) 6292.
- [33] (a) M.U. Anwar, A.S. Elliott, L.K. Thompson, L.N. Dawe, S. Affiliations, *Dalton Trans.* 40 (2011) 4623;  
(b) Z. Xu, L.K. Thompson, D.O. Miller, *J. Chem. Soc., Dalton Trans.* (2002) 2462;  
(c) S. Roy, T.N. Mandal, A.K. Barik, S. Pal, R.J. Butcher, M.S. El Fallah, J. Tercero, S.K. Kar, *Dalton Trans.* (2007) 1229;  
(d) L.N. Dawe, T.S.M. Abedin, T.L. Kelly, L.K. Thompson, D.O. Miller, L. Zhao, C. Wilson, M.A. Leech, J.A.K. Howard, *J. Mater. Chem.* 16 (2006) 2645.
- [34] (a) M.A. Halcrow, *Chem. Soc. Rev.* 42 (2013) 1784;  
(b) H. Hosseini-Monfared, R. Bikas, R. Szymczak, P. Aleshkevych, A.M. Owczarzak, M. Kubicki, *Polyhedron* 63 (2013) 74.
- [35] C. Janiak, *J. Chem. Soc., Dalton Trans.* (2000) 3885
- [36] A. Bencini, D. Gatteschi, *Electron Paramagnetic Resonance of Exchange Coupled Systems*, Springer-Verlag, 1990.
- [37] I. Dzyaloshinsky, *Phys. Chem. Solids* 4 (1958) 241.
- [38] J.W. Orton, *Electron paramagnetic resonance, An introduction to transition group ions in crystals*, Iliffe books Ltd., London, 1968.
- [39] A. Chakraborty, K.L. Gurunatha, A. Muthulakshmi, S. Dutta, S.K. Pati, T.K. Maji, *Dalton Trans.* 41 (2012) 5879.
- [40] (a) A. Jana, S. Konar, K. Das, S. Ray, J.A. Golen, A.L. Rheingold, M.S. El Fallah, S. Mukherjee, S. Gupta, A.J.L. Pombeiro, S.K. Kar, *Polyhedron* 62 (2013) 51;  
(b) H. Hosseini-Monfared, E. Pousaneh, S. Sadighian, S.W. Ng, E.R.T. Tiekink, *Z. Anorg. Allg. Chem.* 639 (2013) 435.
- [41] (a) H. Hosseini-Monfared, R. Bikas, P. Mayer, *Inorg. Chim. Acta* 363 (2010) 2574;  
(b) H. Hosseini-Monfared, R. Bikas, P. Mahboubi-Anarjan, S.W. Ng, E.R.T. Tiekink, *Z. Anorg. Allg. Chem.* 640 (2014) 243;  
(c) H. Hosseini-Monfared, R. Bikas, P. Mahboubi-Anarjan, A.J. Blake, V. Lippolis, N.B. Arslan, C. Kazak, *Polyhedron* 69 (2014) 90.